Target Location Using Dual Beam Directional Modulated Circular Array

Fusco, V., Chepala, A., & Abbasi, M. A. B. (2018). Target Location Using Dual Beam Directional Modulated Circular Array. *IEEE Transactions on Antennas and Propagation*. https://doi.org/10.1109/TAP.2018.2869257

Published in:
IEEE Transactions on Antennas and Propagation

Document Version:
Peer reviewed version

Queen's University Belfast - Research Portal:
Link to publication record in Queen's University Belfast Research Portal

Publisher rights
© 2018 IEEE.
This work is made available online in accordance with the publisher's policies. Please refer to any applicable terms of use of the publisher.

General rights
Copyright for the publications made accessible via the Queen's University Belfast Research Portal is retained by the author(s) and / or other copyright owners and it is a condition of accessing these publications that users recognise and abide by the legal requirements associated with these rights.

Take down policy
The Research Portal is Queen's institutional repository that provides access to Queen's research output. Every effort has been made to ensure that content in the Research Portal does not infringe any person's rights, or applicable UK laws. If you discover content in the Research Portal that you believe breaches copyright or violates any law, please contact openaccess@qub.ac.uk.

Download date:06. May. 2023

This is the author's version of an article that has been published in this journal. Changes were made to this version by the publisher prior to publication.
The final version of record is available at http://dx.doi.org/10.1109/TAP.2018.2869257

Target Location Using Dual Beam Directional Modulated Circular Array

Vincent Fusco, Anil Chepala, M. Ali Babar Abbasi

***Abstract*— A new concept directed towards the location of an object within a sector of space is introduced, by using a combination of the properties associated with directional modulation when implemented on a circular antenna array. In particular, we show that a circular antenna array can be made to project orthogonal data streams on orthogonal spatial beams and through this process create a temporal and spatial interference pattern that can be used for target location. This is demonstrated by way of simulation of a two beam sixteen element circular antenna array carrying QPSK data.**

***Index Terms*— Circular array, directional modulation (DM), phase-shift keying (PSK), physical-layer secure communication.**

I. Introduction

Directional Modulation (DM), is a transmitter technology that is capable of projecting digitally modulated information signals into pre-specified spatial directions while simultaneously distorting the constellation formats of the same signals in all other directions, [1]. Thus affording a level of physical layer security.

Fig. 1 shows a DM system modulated for quadrature phase-shift keying (QPSK). From this figure it can be seen that the standard formatted QPSK constellation patterns, in In-phase and Quadrature (IQ) space, are not preserved along spatial directions away from the pre-defined observation direction $\phi°$ (along azimuth plane), making it difficult for potential eavesdroppers to intercept.

In [2] a DM method which mapped encoded orthogonal I, Q data streams onto two different antenna far field patterns was given. This method was called the dual-beam DM technique and allowed from a knowledge of the two far field patterns projected from the array the transmitted symbol sequence to be decoded only along the two pre-defined directions where the two far field patterns have the same magnitude response. It was shown in [3] that a circular antenna array can be made to project multiple far field beam patterns when suitably excited, for example using a Butler Matrix. This leads to the interesting possibility that a circular antenna array can be made to project the two orthogonal beams each of which can be separately encoded. This approach adds additional flexibility as well as grossly simplifying the practical arrangements in [2] for achieving the same result. In addition, circular arrays have another very useful property. Namely, by offsetting the phases applied to the Butler Matrix exciting the circular array the resulting far field patterns can be made to rotate through 360° in azimuth without the beam shapes distorting [4].

In this paper we show that by co-locating the transmitter and receiver at the phase center of a circular array we can devise a radio location strategy wherein bit error rate (BER) can be used as an indicator of the presence of a target in a given sector of the radar's field of view, while preserving (i) the ability to track the target as it moves in azimuth (ii) general target surveillance. Section II describes the main properties of the circular array and the dual beam DM approach that are relevant to this paper. Section III discusses the far field radiation features based on numerical simulation results for an example 16 element circular array. The resulting IQ spatial trajectory loci and associated BER are also discussed from which target location can be found. Two cases are examined (i) symmetrical beam overlay and (ii) asymmetrical beam overlay. Section IV discusses the tracking characteristics of the circular array based system when the transmitter and the receiver are co-located at each array element, monostatic radar fashion, while the findings are concluded in Section V of the paper.

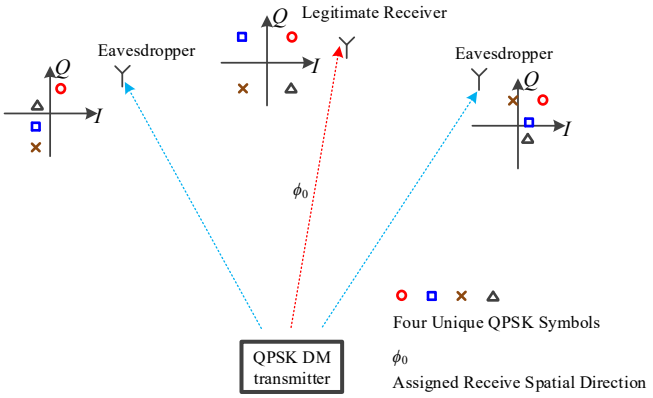

Fig. 1. QPSK DM System Concept, [1].

II. General Circular Array and Dual Beam Directional Modulation Principles

A. General Circular Array Principle

Consider a multimode circular array consisting of 16 half-wavelength dipole antennas. The principle of operation of a multimode circular array is most easily seen by considering a continuous distribution of current, [5]. The horizontal far field directional pattern '$F(\phi)$' of a continuous circular aperture is a periodic function with period 2π. Hence, it can, mathematically be expressed as a complex Fourier series that is a function of both amplitude and phase.

$$F(\phi) = \sum_{m=-M}^{M} C_m e^{jm\phi} \tag{1}$$

where

$$C_m = \int_0^{2\pi} F(\phi) e^{-jm\phi} d\phi \tag{2}$$

When ϕ = azimuth angle and m = mode number. Each of these modes in equation (2) can be excited independently by using a Butler Matrix (BM), [6].

Manuscript received February 5, 2018, revised XXX, published XXX (projected). This work was supported by Queens's University of Belfast Studentship, and the UK Engineering and Physical Science Research Council (EPSRC) under Grant EP/N020391/1.

V. Fusco, A. Chepala, and M. A. B. Abbasi are with The Centre for Wireless Innovation (CWI), The Institute of Electronics, Communications and Information Technology (ECIT), School of Electronics, Electrical Engineering and Computer Science (EEECS), Queen's University Belfast, Belfast BT3 9DT, United Kingdom (email: v.fusco@ecit.qub.ac.uk, achepala01@qub.ac.uk, m.abbasi@qub.ac.uk).

Color versions of one or more of the figures in this communication are available online at http://ieeexplore.ieee.org.
Digital Object Identifier 10.1109/TAP.2018.xxx

Copyright (c) 2018 IEEE. Personal use is permitted. For any other purposes, permission must be obtained from the IEEE by emailing pubs-permissions@ieee.org.

This is the author's version of an article that has been published in this journal. Changes were made to this version by the publisher prior to publication.
The final version of record is available at http://dx.doi.org/10.1109/TAP.2018.2869257

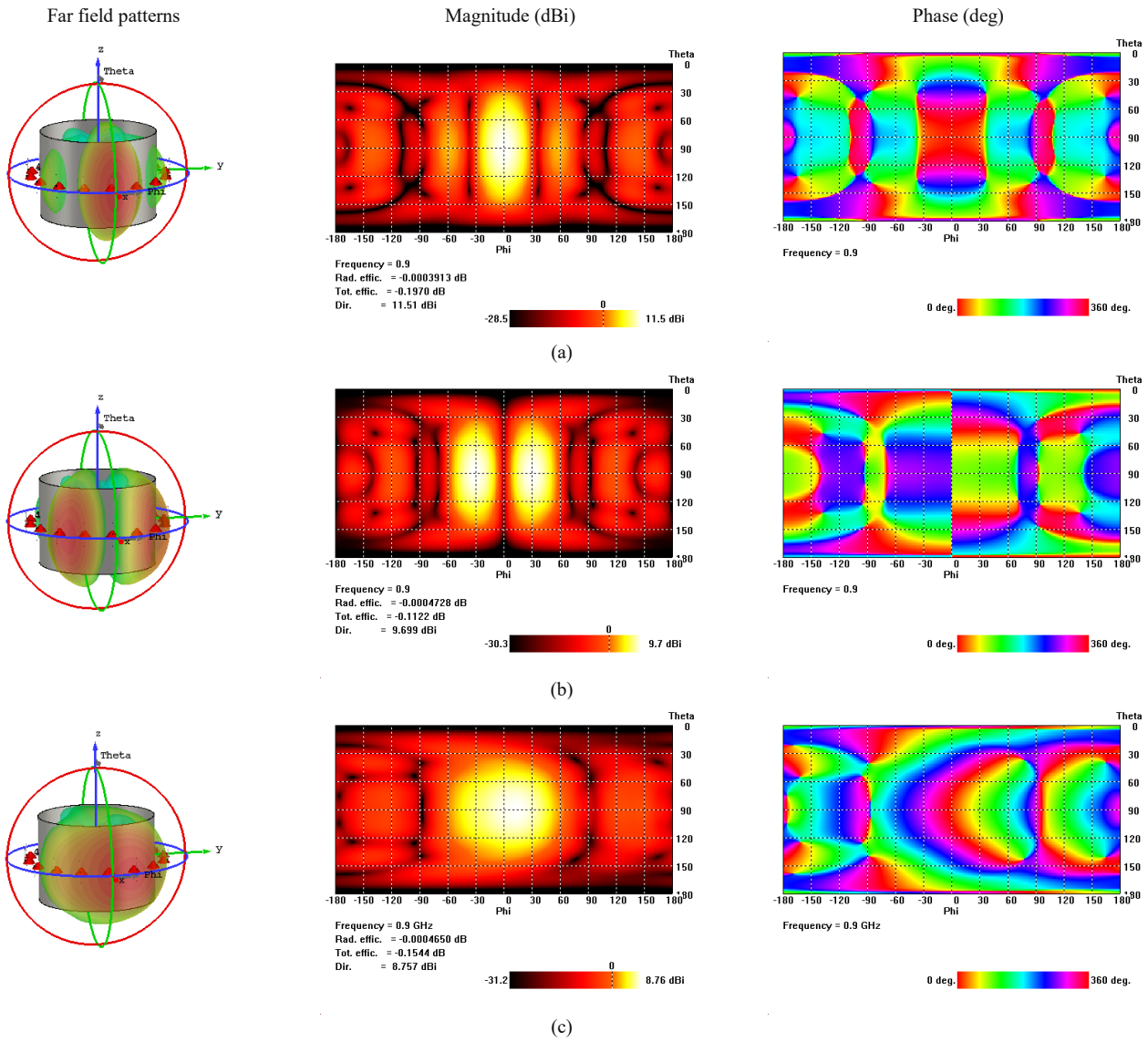

Fig. 2. (a) Sum (Σ), (b) Difference (Δ), and (c) Composite patterns of 16 element circular array at 900MHz. Far field patterns (left), magnitude (center), and phase (right) are displayed column wise.

TABLE I
ANTENNA ELEMENT EXCITATION FOR Σ AND Δ FAR FIELD PATTERNS

Element index	1	2	3	4	5	6	7	8	9	10	11	12	13	14	15	16
|Σ|	0.979	0.666	0.642	0.365	0.227	0.389	0.279	0.339	0.279	0.389	0.227	0.365	0.642	0.666	0.979	1.852
∠Σ	38.6°	157.3°	-164.4°	-77.3°	-81.6°	-164.1°	-130.1°	-70.3°	-130.1°	-164.1°	-81.6°	-77.3°	-164.4°	157.3°	38.6°	23.2°
|Δ|	1.408	1.173	0.592	0.308	0.308	0.173	0.268	0	0.268	0.173	0.308	0.308	0.592	1.173	1.408	0
∠Δ	-73.7°	-56.3°	9.5°	33.4°	-83.3°	-58.7°	56°	52.7°	-124°	121.3°	96.7°	-146.6°	-170.5°	123.7°	106.3°	74.2°

If $B_K e^{j\beta_K}$ is the current applied to the Kth input port, the resultant $A_J e^{j\psi_J}$ on the Jth radiating element is given by

$$A_J e^{j\psi_J} = \frac{B_K e^{j\beta_K} e^{jKJ\left(\frac{2\pi}{N}\right)}}{\sqrt{N}} \tag{3}$$

When many inputs are simultaneously excited then the output current distribution is the summation over K for N element array. The far field radiation pattern assuming the approximate pattern of dipole $A(\phi)$ as $0.5\times(1+\cos(\phi))$ is given by

$$E(\phi) = \sum_J \left[\sum_K B_K e^{j\beta_K} e^{jKJ(2\pi/N)} \right] \cdot A(\phi - \alpha_J) e^{j(\beta r)\cos(\phi - \alpha_J)} \tag{4}$$

When $\beta = 2\pi/\lambda$, λ is the wavelength of operation, and r is the radius of the array, α_J is a general representation of element angular location in a circular array with N equally spaced elements at $\alpha_J = J2\pi/N$, when $J = 1,2, \ldots N$. Referring to the circular array center, the relative phase of the Jth element in this case would be $(2\pi r/\lambda)\cos(\phi - \alpha_J)$.

B Dual Beam Directional Modulation Principle

Copyright (c) 2018 IEEE. Personal use is permitted. For any other purposes, permission must be obtained from the IEEE by emailing pubs-permissions@ieee.org.

This is the author's version of an article that has been published in this journal. Changes were made to this version by the publisher prior to publication.
The final version of record is available at http://dx.doi.org/10.1109/TAP.2018.2869257

In dual beam DM, [2], two excitation signals $s_1(t) = \sigma(t)\times\sin\omega t$ and $s_2(t) = \delta(t)\times\cos\omega t$ are used to encode two transmit beams $F_\Sigma(\phi)$ and $F_\Delta(\phi)$, respectively, where $\sigma(t)$ and $\delta(t)$ define the I and Q channel data information, ω is the carrier frequency, and ϕ is the azimuth angle of the receiver.

According to [2], the receive signal can be expressed as

$$\begin{aligned} E(t,\phi) &= \begin{bmatrix} F_\Sigma(\phi)e^{-j\Phi} & F_\Delta(\phi)e^{-j\Phi} \end{bmatrix} \begin{bmatrix} s_1(t) \\ s_2(t) \end{bmatrix} \\ &= \sigma(t)F_\Sigma(\phi)\cos(\omega t+\Phi) + \delta(t)F_\Delta(\phi)\sin(\omega t+\Phi) \\ &= \Lambda(\phi)\cos\left[\omega t - \Psi(\phi) + \Phi\right] \end{aligned} \tag{5}$$

Here $E(t, \phi)$ is a complex digital symbol with a magnitude and a phase that can be viewed as a constellation point on the real-imaginary coordinate system. Φ is the calibrated RF phase delay defined as $\Phi = \Phi_{Rx} + \Phi_{Cal} + \Phi_{Rot}$. Here, Φ_{Rx} is the instantaneous phase of an RF wave, Φ_{Cal} defines the azimuthal angle dependent phase calibration, while Φ_{Rot} is the phase calibration to prevent rotation of the received constellation. Hence the magnitude and the phase of the receive signal, are respectively,

$$\Lambda(\phi) = \sqrt{F_\Sigma^2(\phi) + F_\Delta^2(\phi)} \tag{6}$$

$$\Psi(\phi) = \tan^{-1}\frac{\delta(t)F_\Delta(\phi)}{\sigma(t)F_\Sigma(\phi)} \tag{7}$$

From which the QPSK symbol transmitted can be decoded at the receiver along an azimuthal direction ϕ. Target location using this QPSK information is detailed in the proceeding sections.

III. Single Cylinder Circular Array

Next we consider what happens when we project two orthogonal far field patterns along direction ϕ. Sum and difference patterns are respectively encoded with the orthogonal I and Q streams of a QPSK symbol set. A Σ and Δ pattern can now be transmitted by the multimode circular array sequentially. At the receive side, the received signal can recreate the transmitted I and Q stream after phase calibration. The sum pattern is characterized by a single main lobe whose cross section is essentially elliptical, while the difference pattern is characterized by a pair of main lobes of opposite phase separated by a single null [7], [8]. The radius of the metal cylinder on which the array is formed is 340 mm. The array has 16 equally spaced half wavelength dipole elements, each tuned for 900MHz operation, and positioned one-quarter wavelength above the metal cylinder at a height of 83 mm. The array excitation matrix (output of BM) for sum and difference patterns is tabulated in Table I when in addition to mode 0, ±4 modes [5] (total 9) are excited. Fig. 2 shows the 3-D sum, difference and composite far field patterns for the example case 16 Element Circular Array when operated at 900 MHz and with the beam maximum for the sum pattern, and the beam null for the difference pattern aligned along $\phi = 0°$.

Fig. 2(b) and (c) presents 2-D representations of 3-D far field patterns, here sum, difference and composite plots are shown from top to bottom. A directive beam at $\phi = 0°$ is evident in the sum plot. Here 2-D contour color intensity represents gain value. Similarly, a far field null at $\phi = 0°$ spreading across the entire elevation plane can be seen from the difference plot in Fig. 2(b). The corresponding phase shows an abrupt discontinuity at $\phi = 0°$ at the position of null. Fig. 3(c) shows the resultant composite patterns for which array excitation is defined as "Σ+Δ". An unequal field distribution along ϕ and θ is evident from Fig. 2(c). 1-D azimuthal cuts of 2-D far field plots are presented in Fig. 3(a). Assuming ideal operation i.e. one in which noise and RF delay are not considered, then at the receiver side, Fig. 3(b) presents the IQ trajectory locus as a function of azimuth angle (ϕ). It is

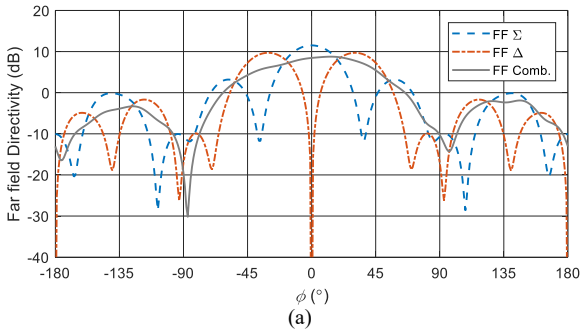

(a)

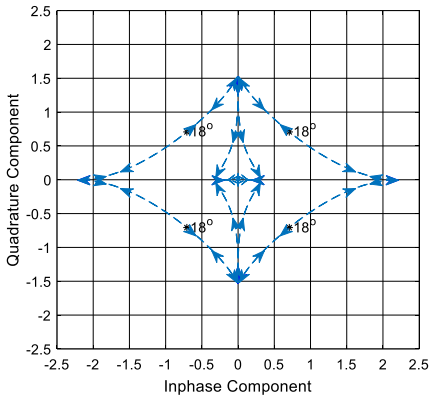

(b)

Fig. 3 (a) Azimuthal cut of far field patterns using Σ (main beam along $\phi = 0°$), Δ (null along $\phi = 0°$) and resultant excitations for 16 element example array. (b) Recovered IQ trajectory locus with azimuthal angle.

interesting to note that the I Q points are located at different Euclidean distances depending on the azimuth angle, as per (1). Since there are two cross over points, in this case symmetrically positioned at ±18°, these will be the spatial locations where the dual DM method will yield the optimum direction for data recovery, i.e. the directions for lowest BER. To further elaborate this, consider all four symbol states of QPSK. Here the sum and difference far-field patterns at the receiver end inherently contain all of the information required to evaluate $\Lambda(\phi)$. On the other hand, $\Psi(\phi)$ depends not only on $F_\Sigma(\phi)$ and $F_\Delta(\phi)$, but also on the instantaneous phase of the received signal. In the absence of noise and RF delay, Φ, when $F_\Sigma(\phi) = F_\Delta(\phi)$, respective symbols will be located on a circle relatively at 0°, 90°, 180° or 270°. In all other cases where $F_\Sigma(\phi) \neq F_\Delta(\phi)$, consecutive symbols' Euclidian distance will disorder depending upon the power and the degree of the difference between $F_\Sigma(\phi)$ and $F_\Delta(\phi)$. This will have a direct impact on BER. For the case presented in Fig. 3(a), $F_\Sigma(\phi) = F_\Delta(\phi)$ occurs at $\phi = \pm 18°$, hence yielding the optimal azimuthal directions for best data recovery. Based on the nearest-neighbor approximation of QPSK constellation, the probability of symbol error rate in [9] is given by:

$$P_s \approx 2Q\left(\frac{d_i/2}{\sqrt{N_0/2}}\right) \tag{8}$$

Where $Q(x)$ is the complementary Gaussian error function, d_i (i=1,2,3,4) is the minimum distance between two constellation points and $N_0/2$ is the noise power spectral density. Considering Gray coding for the four constellation symbols, where each symbol represents two bits, we know that $P_b \approx P_s/2$. Since any QPSK symbol is equally-likely we can predict the probability of bit error along ϕ by:

Copyright (c) 2018 IEEE. Personal use is permitted. For any other purposes, permission must be obtained from the IEEE by emailing pubs-permissions@ieee.org.

This is the author's version of an article that has been published in this journal. Changes were made to this version by the publisher prior to publication.
The final version of record is available at http://dx.doi.org/10.1109/TAP.2018.2869257

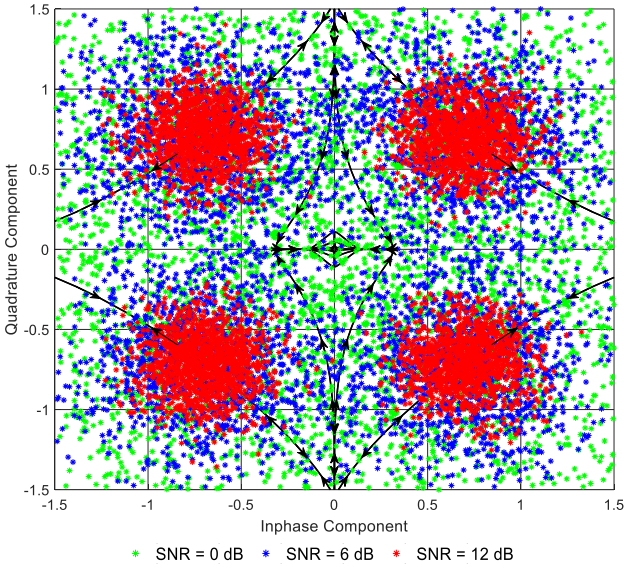

Fig. 4. Computed constellation diagrams under the presence of Noise at multiple SNR levels along the azimuth direction $\phi = +18°$.

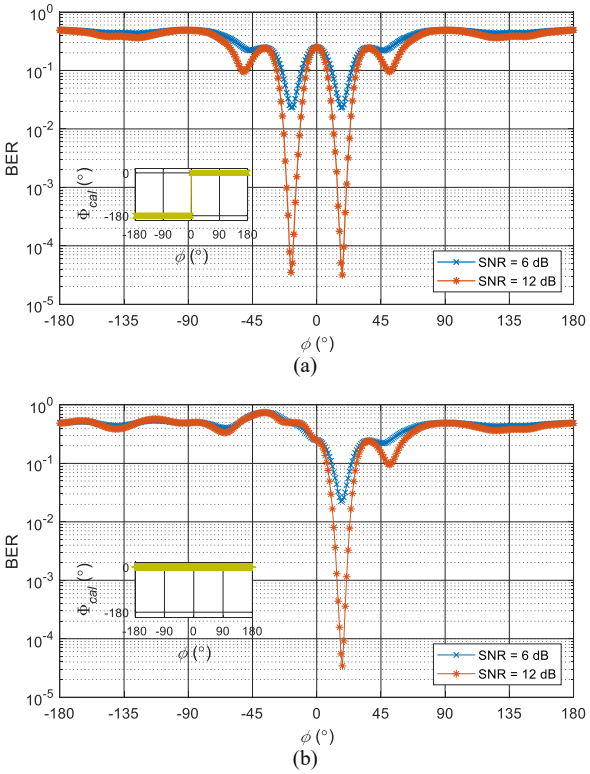

Fig. 5. Computed BER as a function of azimuthal angle for symmetric Σ, and Δ patterns in the (a) presence and the (b) absence of the phase calibration Φ_{Cal}.

$$P_b(error) \approx \frac{1}{4}\left[Q\left(\sqrt{\frac{F_\Sigma^2(\phi)}{N_0}}\right) + Q\left(\sqrt{\frac{F_\Delta^2(\phi)}{N_0}}\right)\right] \quad (9)$$

Fig. 4 shows the situation when noise is added to the data. From this it can be seen that, as expected, as SNR increases then the constellations become better defined along the ±18° directions in this case. Next we compute the BER for the system, here for example,

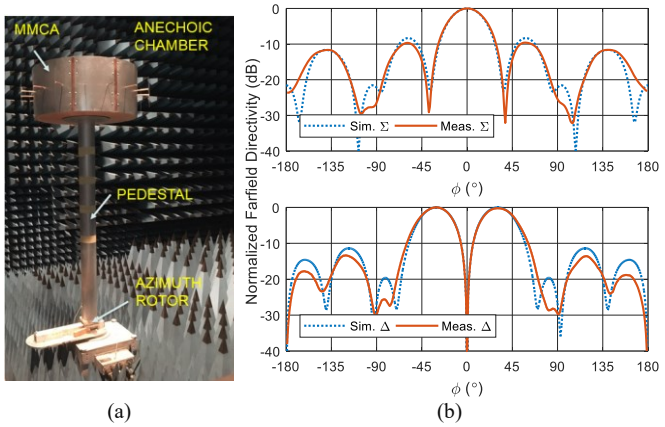

Fig. 6 (a) Fabricated MMCA and experimental setup photograph. (b) Comparison between measured and simulated far field patterns along azimuthal cut using Σ (main beam along $\phi = 0°$) and Δ (null along $\phi = 0°$) excitations for 16 element example array.

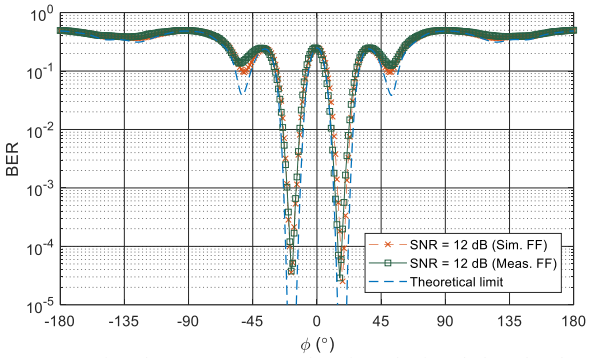

Fig. 7. Comparison between BER as a function of azimuthal angle when BER is computed based on the simulated and measured far field patterns. Theoretical BER limit is defined by equation (9).

when SNR = 6dB and when SNR = 12dB as a function of azimuth angle. A simulation campaign is carried out in which the circular array, operating at 900 MHz, transmits a data stream of 10 million ideal random bits, to ensure the simulated BER accuracy up to 10^{-4}. The results are presented in Fig. 5. The instantaneous phase of an RF wave needs a re-calibration at the receiver end to form an un-rotated constellation like the one presented in Fig. 4. Fig. 2(a) and (b) identify an azimuth and elevation sector in which the phase of the RF wave is almost the same. For both Σ and Δ patterns, the phase remains almost constant within the elevation direction $60° < \theta < 120°$. From Fig. 2(b), if we compare the phases along the two azimuthal directions i.e. -180° $\leq \phi \leq$ 0° and 0° $< \phi \leq$ 180°, it can be seen that the two phases are 180° apart. Fig. 5. shows that when this difference is calibrated, BER has a clear spatial preference along the ±18° directions. (see Fig. 5(a)). On the other hand, when this difference is not calibrated, it will eventually result in a high BER at ϕ = -18° and low BER point the azimuth direction $\phi = +18°$, reducing two BER minima to one BER minima along the azimuthal angle (see Fig. 5(b)). This is because of the fact that for the azimuthal direction -180° $\leq \phi \leq$ 0°, the receiver will see a 180° rotation in the entire constellation when the complex digital symbol $E(t, \phi)$ is constructed, eventually resulting in a high BER.

IV. Experimental Results

To demonstrate the practical implementation of the proposed scheme, multimode circular array (MMCA) is fabricated and far field

Copyright (c) 2018 IEEE. Personal use is permitted. For any other purposes, permission must be obtained from the IEEE by emailing pubs-permissions@ieee.org.

This is the author's version of an article that has been published in this journal. Changes were made to this version by the publisher prior to publication.
The final version of record is available at http://dx.doi.org/10.1109/TAP.2018.2869257

response is evaluated in an anechoic environment. Each of the 16 radiating elements of the MMCA are designed to operate at 0.9 GHz. The MMCA consists of 16 half-wavelength dipole antennas each fed by a quarter wavelength balun and arranged around a circle of diameter 848 mm. The metallic cylinder diameter is 680 mm, height is 300 mm and thickness is 2 mm. The dipoles are separated from the metallic cylinder by a distance of 83 mm. The dipoles are uniformly deployed and the separation angle between the consecutive dipoles is 22.5°. Detailed information on the impact of a circular array size, radius and number of elements can be found in [5]. Experimental setup and measured far field patterns are presented in Fig. 6 depicting good agreement with the predictions. These measured patterns are post processed to estimate the BER performance along the azimuthal direction. The results (presented in Fig. 7) verify the proposed dual beam directional modulation principle for target location and tracking.

System generated phase noise while simultaneous excitation of antenna array elements is inevitable. In order to evaluate the impact of phase noise on the far field directivity, a simulation campaign was carried out based on the measured phase noise data. Random phase noise with a measured standard deviation of 2° and variance of 4° was introduced into the excitation matrix of the 16 element circular array. As a result, deviance of < 0.5 dB and $< \pm 2°$ was observed in $|F(\phi)|$ and $\angle F(\phi)$ respectively. This deviation has a slight impact on the BER performance, for example, consider the measured far field with an SNR = 12 dB, the BER value at $\phi = +18°$ went from 3.77×10^{-5} to 3.40×10^{-5} in the presence and the absences of the deviations.

One of the main advantage of the circular array is that the mutual coupling among the elements is rotationally symmetric [5]. This ensures a symmetric beam scan with very small variation in gain and beam shape. The patterns projected in the graphs presented in Fig. 2, 3(a) and 6(b) include the effects of the mutual coupling.

V. Tracking Application

If the transmitter and the receiver are co-located, then the values required for evaluation of (1) are available. For example, expected received power is deducible from the transmitted $F_\Sigma(\phi)$ and $F_\Delta(\phi)$ in Fig. 3(a), and can be used to evaluate constellation (Fig. 4) at an expected azimuthal direction ϕ. In addition, since the data transmission sequence is known then BER can be readily calculated. Examination of Fig. 3 shows that while target illumination occurs over a wide field of view, altering to the presence of a target, the computed BER, according to Fig. 5 will only drop to a very low value when the target is aligned with the DM directions, in this case ±18°. In this way the sector in which the target lies can be identified. Target ranging can also follow by using time of arrival (TOA) based measurements with an appropriate symbol sequence. In Fig. 3 the composite pattern half power beam width (HPBW) is 78.5° while the DM beam width defined as the angle between the BER values of $<10^{-3}$ is 7.5° so that, in a sense, the DM arrangement digitally enhances the directivity of the system.

Next we recall that since we are using a circular array with electronic beam scanning ability, we can easily rotate both beams synchronously. This allows the possibility to track the location of the target as it moves in azimuth around the system permitting 360° coverage. Similarly, we could oscillate the composite beam $\pm\ \phi°$ in order to determine target direction of travel. Further, if we wished to communicate data to a target equipped with a suitable receiver we could achieve this through the IQ payload. In addition to the above features, once the target is located within a sector we can un-balance the system by skewing the difference pattern location with respect to the sum pattern. This situation is shown in Fig. 8. Here the difference

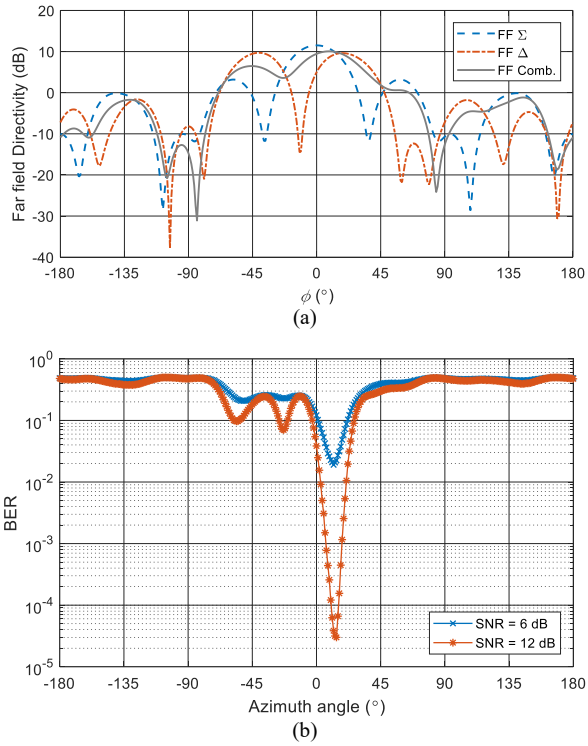

Fig. 8. Asymmetrical condition (a) Azimuthal cut Sum, Difference and Resultant far field patterns for 16 element example array. (b) Computed BER as a function of azimuthal angle.

pattern null is shifted to –12° the result of which is to significantly un-balance the DM in the $-\phi°$ direction while preserving the $+\phi°$ direction. Consequently, the resulting system shows a single DM direction which could, for example, now together with beam rotation be used for unique target position location. Following this, the sum pattern could be switched off, and the difference pattern null steered onto the target as this would yield better positional estimation since from Fig. 3 the difference pattern beam width at -20dB is $< 5°$ while the asymmetrical BER BW is 11.5° for 10^{-3} BER. Physical layer security and concurrent data communication are added benefits of the proposed scheme, enabling a possibility of not only tracking, but also establishing a secure communication with a target using IQ payload.

VI. Conclusion

In this paper we show a new concept which relies on the concurrent multiple beam and beam rotation properties of a circular array coupled with the dual directional modulation coding scheme. In this way the feasibility of tracking a non-cooperative target has been established. The additional possibility of communicating with a suitable receiver equipped target was also described. The technique may therefore be useful in a variety of scenarios, such as, where bandwidth is a premium, full azimuthal coverage is required, or communication to a target is needed while tracking its movement.

Acknowledgment

This work was supported by a Queens's University of Belfast Studentship, and by EPSRC grant EP/N020391/1.

References

[1] Y. Ding and V. F. Fusco, "A vector approach for the analysis and synthesis of directional modulation transmitters," *IEEE Trans.*

Copyright (c) 2018 IEEE. Personal use is permitted. For any other purposes, permission must be obtained from the IEEE by emailing pubs-permissions@ieee.org.

This is the author's version of an article that has been published in this journal. Changes were made to this version by the publisher prior to publication.
The final version of record is available at http://dx.doi.org/10.1109/TAP.2018.2869257

Antennas Propag., vol. 62, no. 1, pp. 361–370, 2014.

[2] T. Hong, M.-Z. Song, and Y. Liu, "Dual-beam directional modulation technique for physical-layer secure communication," *IEEE Antennas Wirel. Propag. Lett.*, vol. 10, pp. 1417–1420, 2011.

[3] C. Sudrez-Fajardo, M. Ferrando-Batallur, A. Valero, and V. Rodrigo, "Multiple beam system with circular arrays," in *Antennas and Propagation Society International Symposium, 2005 IEEE*, 2005, vol. 4, pp. 35–38.

[4] D. E. N. Davies and B. S. McCartney, "Cylindrical arrays with electronic beam scanning," in *Proceedings of the Institution of Electrical Engineers*, 1965, vol. 112, no. 3, pp. 497–505.

[5] B. Sheleg, "A matrix-fed circular array for continuous scanning," *Proc. IEEE*, vol. 56, no. 11, pp. 2016–2027, 1968.

[6] H. Moody, "The systematic design of the Butler matrix," *IEEE Trans. Antennas Propag.*, vol. 12, no. 6, pp. 786–788, 1964.

[7] M. I. Skolnik, "Radar handbook," 1970.

[8] R. Elliott, "Array pattern synthesis," *IEEE Antennas Propag. Soc. Newsl.*, vol. 27, no. 5, pp. 4–9, 1985.

[9] A. Goldsmith, *Wireless communications*. Cambridge university press, 2005.

Copyright (c) 2018 IEEE. Personal use is permitted. For any other purposes, permission must be obtained from the IEEE by emailing pubs-permissions@ieee.org.